2005-01-17

Nuclear transport of single molecules: dwell times at the nuclear pore complex

Ulrich Kubitscheck
Westfalische Wilhelms-Universitat

Et al.

Published January 18, 2005

Nuclear transport of single molecules: dwell times at the nuclear pore complex

Ulrich Kubitscheck, David Grünwald, Andreas Hoekstra, Daniel Rohleder, Thorsten Kues, Jan Peter Siebrasse, and Reiner Peters

Institute of Medical Physics and Biophysics, Westfälische Wilhelms-Universität, D-48149 Münster, Germany

The mechanism by which macromolecules are selectively translocated through the nuclear pore complex (NPC) is still essentially unresolved. Single molecule methods can provide unique information on topographic properties and kinetic processes of asynchronous supramolecular assemblies with excellent spatial and time resolution. Here, single-molecule far-field fluorescence microscopy was applied to the NPC of permeabilized cells. The nucleoporin Nup358 could be localized at a distance of 70 nm from POM121-GFP along the NPC axis. Binding sites of NTF2, the transport receptor of RanGDP, were observed in cytoplasmic filaments and central framework, but not nucleoplasmic filaments of the NPC. The dwell times of NTF2 and transportin 1 at their NPC binding sites were 5.8 ± 0.2 and 7.1 ± 0.2 ms, respectively. Notably, the dwell times of these receptors were reduced upon binding to a specific transport substrate, suggesting that translocation is accelerated for loaded receptor molecules. Together with the known transport rates, our data suggest that nucleocytoplasmic transport occurs via multiple parallel pathways within single NPCs.

Introduction

Nucleocytoplasmic transport is mediated by the nuclear pore complex (NPC), a large transporter spanning the nuclear envelope (NE; for review see Fahrenkrog and Aebi, 2003). In yeast (Yang et al., 1998) and vertebrates (Fahrenkrog and Aebi, 2002), the NPC has a highly symmetrical structure. A cylindrical central framework of octagonal symmetry, measuring ~120 nm in diameter and 70 nm in length, is decorated by eight cytoplasmic filaments of ~50 nm length, while eight nuclear filaments of ~150 nm in length connect at their tips to form a basket. The NPC is made up of ~30 different polypeptides (Rout et al., 2000; Cronshaw et al., 2002) referred to as nucleoporins, which occur in multiples of eight to yield a total mass of ~40 MD (yeast) or ~60 MD (vertebrates). About one third of the nucleoporins contain repetitive sequences (FG repeats) in which the residues FG, GLFG, or FxFG are separated by hydrophilic linkers of variable length.

The NPC supports at least three distinct types of transport: restricted diffusion, facilitated diffusion, and unidirectional Ran-dependent transport (Suntharalingam and Wente, 2003). Molecules, which do not specifically interact with nucleoporins and in that sense are inert, permeate the NPC at rates inversely related to their molecular size. Transport rates are consistent with restricted diffusion through a channel within the NPC center ~10 nm in diameter and ~45 nm in length (Peters, 1986; Keminer and Peters, 1999). In contrast, the translocation of molecules, which specifically interact with FG repeats of nucleoporins such as the transport receptors transportin 1/karyopherin β2 (Pollard et al., 1996; Bonifaci et al., 1997), NTF2/p10 (Moore and Blobel, 1994; Paschal and Gerace 1995), and NXT1/p15, is facilitated (Ribbeck and Görlich, 2001; Siebrasse and Peters, 2002; Kiskin et al., 2003). For instance, NTF2, a 15-kD monomer forming homodimers, is translocated through the NPC of *Xenopus laevis* oocytes ~10 times faster than α-lactalbumin (14 kD) and ~50 times faster than GFP (29 kD; Siebrasse and Peters, 2002; Kiskin et al., 2003). Substrates containing an NLS do not interact directly with the NPC but bind in cytoplasm to soluble transport receptors. These import complexes are translocated through the NPC and dissociate in the nucleus upon binding of RanGTP. Conversely, substrates containing a nuclear export signal form ternary complexes with a transport receptor and RanGTP in the

Correspondence to Ulrich Kubitscheck: u.kubitscheck@uni-bonn.de

U. Kubitscheck's and D. Grünwald's present address is Institute for Physical and Theoretical Chemistry, University of Bonn, 53115 Bonn, Germany.

D. Rohleder's present address is Institute for Physical Chemistry, Julius-Maximilians-Universität Würzburg, 97074 Würzburg, Germany.

T. Kues's present address is Carl Zeiss Jena GmbH, 50739 Köln, Germany.

Abbreviations used in this paper: EMCCD, electron-multiplying CCD; NE, nuclear envelope; NPC, nuclear pore complex.

The online version of this article includes supplemental material.

Supplemental Material can be found at:
http://jcb.rupress.org/content/suppl/2005/01/18/jcb.200411005.DC1.html

The Journal of Cell Biology, Vol. 168, No. 2, January 17, 2005 233–243
http://www.jcb.org/cgi/doi/10.1083/jcb.200411005

Published January 18, 2005

nucleus, which are translocated through the NPC, and hydrolysis of Ran-bound GTP induces their dissociation.

Restricted and facilitated diffusion through the NPC are passive bidirectional processes. However, the receptor-mediated transport of NLS- and nuclear export signal–containing substrates is vectorial and can proceed against concentration differences. The mechanism by which molecules are translocated through the NPC is essentially unresolved. It is established that transport receptors bind to FG repeats of nucleoporins, and it is thought that this binding facilitates translocation. However, both the topographic arrangement of binding sites within the NPC and the functional relations between binding and transport are a matter of speculation.

Single molecule methods (Michalet et al., 2003) can provide unique information on topographic properties and kinetic processes that is lost by averaging over large populations of unsynchronized molecules. One approach to single-molecule detection that is particularly suited for biological applications is far-field optical microscopy using high-sensitivity CCD camera systems (Schmidt et al., 1999). Single molecules are imaged as diffraction-limited spots, which may be approximated by a two-dimensional Gaussian function. At a wavelength of 660 nm and a numerical aperture of 1.4 of the used objective lens the full width at half maximum of the Gaussian is 390 nm. Thus, the shape of a submicroscopic particle cannot be resolved, but the position of the particle can be determined with high precision by a fitting process. The localization precision depends on the signal/noise ratio and, according to numerous theoretical and experimental studies, may reach a few nanometers under optimal conditions (Thompson et al., 2002; Yildiz et al., 2003). Thereby, single molecule detection allows us to follow the traces of single molecules. The technique has mostly been applied to analyze the movement of single receptors and lipid molecules in membranes (for review see Schütz et al., 2000), but was recently extended to study also single-molecule mobility within the interior of mammalian cells (for reviews see Moerner, 2003; Sako and Yanagida, 2003). By using multicolor fluorescence, distances between differently labeled single molecules or structures may be determined with precisions in the range of a few nanometers (van Oijen et al., 1998).

In this work, single-molecule methods were applied to the NPC of digitonin-permeabilized somatic cells. This approach was recently shown to yield significant insight into the understanding of nucleocytoplasmic transport (Kubitscheck, U., A. Hoekstra, T. Kues, J.P. Siebrasse, and R. Peters. American Biophysical Society Meeting. 2003. 123A; Babcock et al., 2004; Yang et al., 2004). Using antibodies, the location of the nucleoporin Nup358 on the axis of the NPC could be resolved at a precision previously achieved by electron microscopy of fixed, embedded, and sectioned specimen only. The distribution of binding sites were analyzed for the nuclear transport receptors NTF2, and the dwell times of the import receptors NTF2 and transportin 1 with and without their respective transport substrates have been measured. The results have profound implications for the mechanism of translocation through the NPC.

Results

Coordinates of the NE can be determined in permeabilized cells at nanometer precision by high-sensitivity fluorescence microscopy

To localize NE and NPCs in permeabilized cells by fluorescence microscopy, we used a HeLa cell line stably expressing a GFP conjugate of the nucleoporin POM121 (Bodoor et al., 1999). POM121 is localized in the center of the NPC as indicated in Fig. 1 (Söderqvist et al., 1997). Fluorescence microscopic images of permeabilized HeLa cells expressing GFP-POM121 (Fig. 2 A) showed the NE as punctuate line. A one-dimensional peak-fitting program was used to determine the positions of the GFP-POM121 with sub-pixel resolution (Fig. 2 B; see Materials and methods and the Online supplemental material for details). The position of the fluorescence maximum could thus be determined with a precision of 10 nm (Kubitscheck et al., 2000). The peak positions of the fits were considered as the centers of the NPCs and used as origin ($x = 0$) of a coordinate system along the NPC axis.

In equatorial optical sections of nuclei, the NPCs were usually not resolved as separate entities. The NPC density was $\sim$5 NPCs/μm^2, so that the nearest neighbor distance between NPCs was $<$0.4 μm (Kubitscheck et al., 1996). The radial and axial resolution of our microscopic setup was 0.3 and 0.8 μm, respectively. Therefore, the signals of single NPCs generally overlapped, especially in the axial direction. Only in regions of the NE having by chance a low NPC density single NPCs could be visualized as single fluorescent spots.

The gross topography of the NPC can be resolved by single-molecule fluorescence microscopy

To study the topography of the NPC, we used Nup358, a major structural component of the cytoplasmic filaments (Wilken et

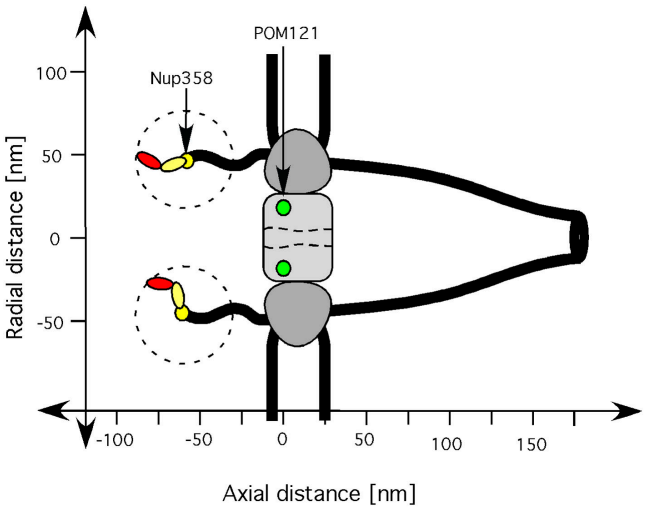

Figure 1. **Topographic markers at the NPC.** Sketch of the site of GFP-POM121 (green), the binding sites of the primary antibody αNup358 (yellow), and the Alexa633-labeled secondary antibody (red). The range of geometrical binding configurations is indicated by the dashed circles, and spreads the experimentally observed label distribution by ±30 nm.

Published January 18, 2005

al., 1995; Wu et al., 1995; Delphin et al., 1997). Immunelectron microscopic studies using an antibody against Nup358 residues 2550–2837 revealed a peak of binding sites at a distance of 59 nm from the NPC mid-plane (Wu et al., 1995). Similarly, an analysis using an antibody against Nup358 residues 2501–2900 yielded a peak at 70 nm from the NPC midplane with a mean distance of 57 ± 11 nm, and a polyclonal antibody against residues 2290–2314 yielded a distance of 51 ± 10 nm, also suggesting that the COOH terminus of that large nucleoporin is oriented toward the cytoplasm (Walther et al., 2002).

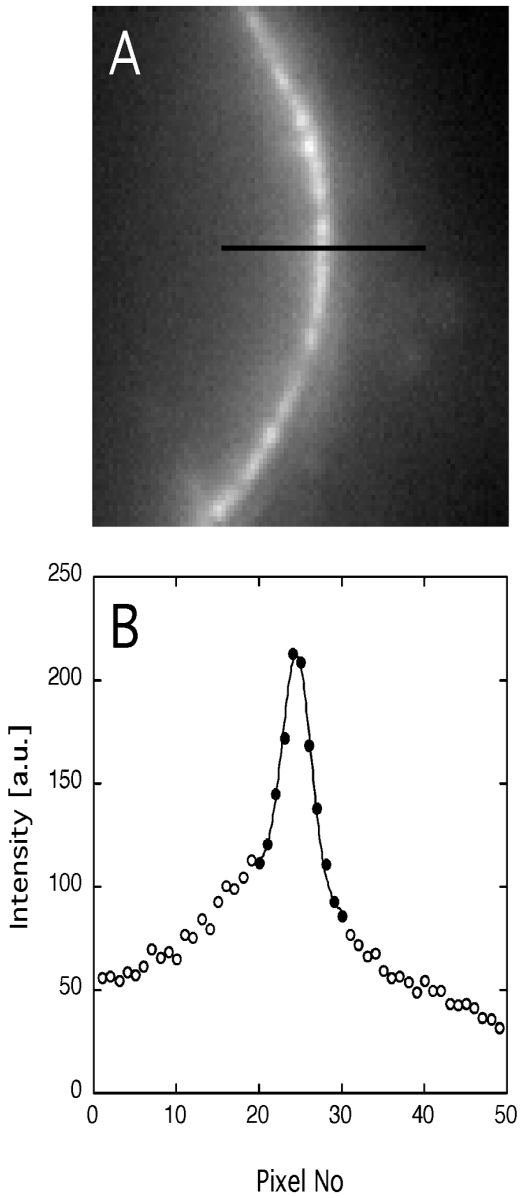

Figure 2. **Labeling of the NE by GFP-POM121.** (A) Bright-field image of the equatorial plane of HeLa cell nucleus. A line of green fluorescence originating from GFP-POM121 contained in the NPCs in focus marked the position of the NE. The image was smoothed using a 5 × 5 Gaussian kernel with a SD of 1 pixel and contrasted for display. Field size, 10.8 × 10.8 μm^2. (B) Profile along a row of pixels (solid line in A), and fitting result on the basis of a Gaussian on a linear ramp in a region of ±5 pixels within the maximum (solid line, closed circles). The unsymmetrical shape of the profile was due to the GFP-POM121 within out-of-focus regions of the NE (left of the NE in A).

We labeled permeabilized HeLa cells expressing GFP-POM121 with the primary polyclonal anti (α)-Nup358 antibody developed by Wu et al. (1995). Then, one channel of the two-color CCD video system was used to acquire a single image of the green GFP-POM121 fluorescence. Subsequently, a red fluorescent secondary antibody was added to the specimen in picomolar concentrations, and the second channel of the video system was used to record an image sequence at 6.7 Hz frame repetition rate and 1 min total length to monitor the appearance and binding of single secondary antibodies at the NE. To achieve optimal localization precision, a single frame integration time of 50 ms was used. After movie acquisition, a further image of POM121 fluorescence was recorded in channel one as stability control. Finally, the two channels were aligned and the position of each antibody molecule was determined in relation to the NE. Fig. 3 A shows selected frames of such an image sequence. Here, the red fluorescence of single antibody molecules was overlaid with the green fluorescence of GFP-POM121.

Image sequences as shown in Fig. 3 A were evaluated by a nonlinear peak-fitting algorithm, which yielded the positions, widths, and relative intensities of the antibody signals (see Online supplemental material, available at http://www.jcb.org/cgi/content/full/jcb.200411005/DC1). The positional precision was 20–40 nm, i.e., far beyond optical resolution. In general, fluorescent antibody molecules could only be observed as diffraction-limited spots when attached to immobile structures (e.g., NPC-bound primary antibodies). Due to the long integration time used in these experiments the signals of freely diffusing antibody molecules were blurred by fast motion and mostly vanished in the background noise. The time for which single secondary antibody molecules were seen at the NE (residence time) varied between 0.15 and 3.0 s (i.e., 1–20 images). The disappearance of antibody molecules was presumably caused by photobleaching or dissociation. Examination of the photostability of the Alexa633-labeled secondary antibodies showed that they could be observed at the applied conditions for 20 images on average. Due to their heterogeneous nature, polyclonal antibodies show a wide range of dissociation rate constants, which may extend from 1 s^{-1} up to 10^{-3} s^{-1} (Kuby, 1994). Therefore, the observed residence times were in the expected range. Furthermore, we compared the fluorescence intensities of putative single antibody molecules in the aforementioned experiments with those from the same molecules attached to the surface of coverslips (unpublished data). On average, the latter signals were 2.6-fold brighter compared with the intracellularly detected signals. A signal reduction of this extent was expected due to scattering effects and the refractive index mismatch between immersion medium and mounting buffer (Hell et al., 1993). This corroborated the assumption that the intracellularly observed diffraction-limited signals were indeed images of single antibody molecules, and not, e.g., aggregates of molecules.

In Fig. 3 B, the outcome of a representative experiment is shown. Dots represent the positions of single antibody molecules while the line indicates the center of the NE as derived from the GFP fluorescence. Conspicuously, many sites along the NE (Fig. 3 B) bound several antibody molecules one after

Published January 18, 2005

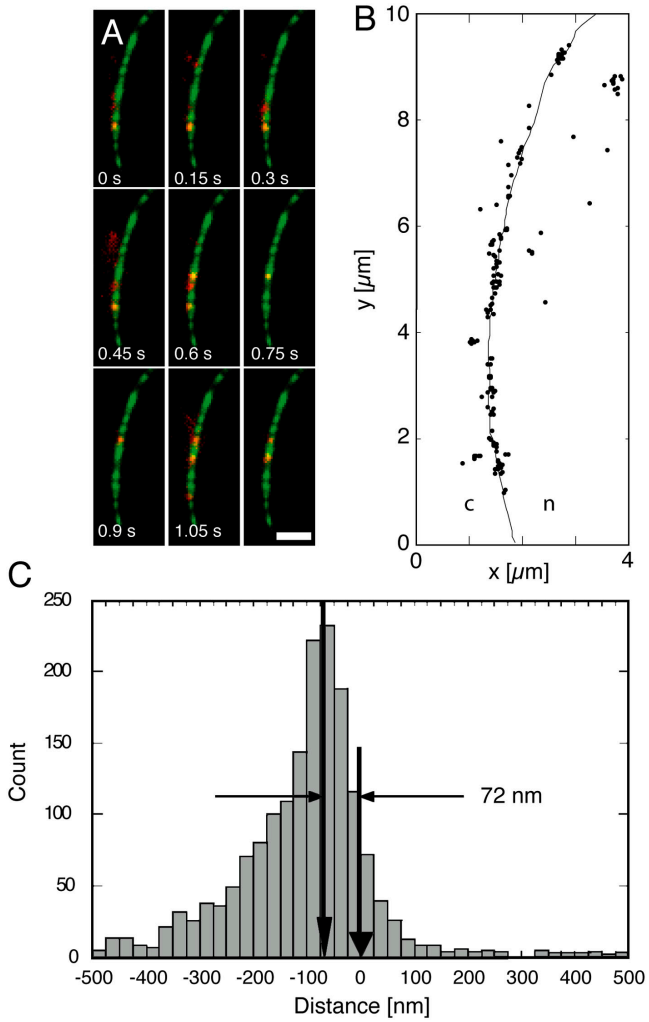

Figure 3. **Observation of single antibodies at the NE.** (A) Single frames of a video sequence showing the binding of secondary Alexa633-labeled antibodies (red spots) to preincubated αNup358 in the equatorial plane of a HeLa cell nucleus. An image of GFP-POM121 was acquired before movie acquisition and overlaid by the red channel image data. It was possible to visualize the binding of individual fluorescent antibodies to their NPC-bound epitopes one at a time. Images were smoothed using a 5 × 5 Gaussian kernel with a SD of 1 pixel and contrasted for display (integration time, 50 ms; frame rate, 6.67 Hz). Bar, 2 μm. (B) Plot of all antibody positions determined in the complete video sequence (400 images). The solid line shows the positions of the GFP-POM121 indicating the NE (c, cytoplasm; n, nucleoplasm). (C) Frequency histogram of the αNup358 binding sites in relation to the respective nearest point of the NE (defined as zero). The histogram has a distinct maximum at d = −72 ± 10 nm (left arrow). The data clearly demonstrate that Nup358 is located at the tips of the cytoplasmic filaments.

the other. These regions had just the extension of an NPC. Thus, in contrast to the simultaneous labeling of NPCs by GFP-POM121, the sequential labeling by antibody molecules presumably made single NPCs visible (Yang et al., 2004). Although an unambiguous identification of single NPCs remained impossible, the estimated density of putative NPCs was consistent with expectation.

The coordinates of the observed antibody binding sites were used to calculate their distances from the NE. The frequency distribution of such distance values, as determined in five experiments, is shown in Fig. 3 C. A clear maximum was found on the cytoplasmic side of the NPC center at d = −72 nm. The distribution was asymmetrical because of occasional unspecific binding of the antibody in the cytoplasm. An extensive discussion of the measurement error analysis is contained in the Online supplemental material. Wu et al. (1995), using the same αNup358 antibody used in this work, localized Nup358 in a fixed electron microscopic specimen at a distance of 59 nm from the NPC mid-plane. Thus, the present results, concerning permeabilized cells in physiological medium, are in good agreement with the previous electron microscopic studies. In control experiments without primary antibodies, no binding of the used secondary antibodies was detected near the NE.

Nuclear transport receptor NTF2 binding sites are distributed throughout the central framework of the NPC

The interaction of NTF2 with the NPC was studied using recombinant Alexa488-labeled human wild-type NTF2. The used NTF2 preparation bound strongly to the NPC of *X. laevis* oocytes and was translocated through the NPC at high rates (Siebrasse and Peters, 2002). In additional experiments, NTF2 labeled by the more photostable Alexa633 was used. Control experiments with unconjugated Alexa488 or Alexa633 showed that neither dye interacted notably with the NPC.

The experimental procedure using Alexa488-labeled NTF2 was as follows: GFP-POM121–expressing HeLa cells were permeabilized and the equatorial plane of a cell nucleus was brought into focus. Then, NTF2-Alexa488 was added at picomolar concentrations. Image sequences were acquired in which the samples were repeatedly illuminated for 50 ms with an irradiance of 2.0 ± 0.5 kW/cm^2 of 488-nm laser light at a lag time of 100 ms between subsequent images. Complete and irreversible bleaching of the GFP fluorescence occurred within an illumination time of 1 s. After that, single Alexa488-labeled NTF2 molecules became visible at the NE. Several video stills from a video sequence (Video 1, available at http://www.jcb.org/cgi/content/full/jcb.200411005/DC1) illustrating this are shown in Fig. 4 A.

The first images of an image sequence were used to determine the position of the NPCs. Later images were used to derive the positions of single NTF2 molecules and to determine their distance from the NPCs. In Fig. 4 B, the positions of NPCs (line) and individual NTF2 molecules (dots) are shown together. Over a 10-μm long stretch of the NE, ∼30 NTF2 binding sites were observed, corresponding to a density of 3–6 NPC/μm^2. The distribution of the distances between individual NTF2 molecules and the NPCs has a narrow, almost symmetrical, shape with a maximum slightly shifted to the cytoplasmic side (x = −30 nm; Fig. 4 C). Notably, the obtained binding site distribution was as narrow as that of a recent electron microscopic study (Bayliss et al., 1999).

Experiments with Alexa633-labeled NTF2 followed a slightly different protocol. After permeabilization of cells and addition of Alexa633-labeled NTF2, the NE was imaged once in the first recording channel. An image series was acquired in the second channel, recording the positions of NTF2 molecules. As

Published January 18, 2005

in the case of Alexa488-labeled NTF2, the majority of NTF2 molecules was detected immediately at the NE and only a few molecules were observed in the nucleus or cytoplasm. Occasionally, NTF2 molecules bound repeatedly to the same site in the cytoplasm, possibly to NPCs in annulate lamellae (Cordes et al., 1997). The distribution of Alexa633-labeled NTF2 was not as narrow as that of Alexa488-labeled NTF2 (Fig. S5, available at http://www.jcb.org/cgi/content/full/jcb.200411005/DC1), a fact that was certainly due to the lower colocalization precision of the dual color fluorescence approach. However, also the distribution of Alexa633-labeled NTF2 had a peak within the NPC center, only slightly shifted toward the cytoplasmic side.

The dwell time of NTF2 at the NPC is 5.8 ms

Experiments on the interaction of NTF2 with the NPC, as described in the previous paragraph, yield not only spatial but also temporal information. To examine the duration of binding events, we performed further experiments at higher time resolution using a fast frame-transfer electron-multiplying CCD (EM-CCD) camera with single frame integration times ranging from 2 to 5 ms with frame rates of 200–500 images/s. To avoid biasing the dwell times by photobleaching, we used for these experiments NTF2 labeled by the photostable Alexa633. NTF2-Alexa633 is also observed predominantly directly at the NE upon addition to digitonin-permeabilized cells (Fig. S5). The resulting high-speed movies (Video 2, available at http://www.jcb.org/cgi/content/full/jcb.200411005/DC1) presented a huge amount of data, and therefore were evaluated using a special data reduction approach, which is detailed in the Online supplemental material. In short, in each frame we evaluated only the fluorescence intensity along the curved line of the NE. These data were plotted as a function of time yielding yt-images showing the events at the NE during the experiment (Fig. 5 A). The appearance of single NTF2 molecules at the NE is indicated in these images by transient horizontal signals. Their lengths along the t-axis documented the duration of the binding events (Fig. 5 B, arrows). In most cases, the binding events were of short duration, in the range of milliseconds only. Genuine binding events were detected in the following way. The background intensity was Gaussian distributed (Fig. 5 C, left peak). Therefore, the probability that a signal with an intensity of mean plus 4 SD is observed is ~0.003%, i.e., it happens in three out of 10^5 measurements by chance. Because our time traces contained up to 10^4 data points, the chance to observe such a signal was virtually zero. Thus, those signals with intensity values greater than the mean plus 4 SD indicated binding events of fluorescent molecules. In cases where long or multiple binding events were observed in a single time trace, the frequency histogram of intensity values displayed even two distinct maxima (Fig. 5 C). The evaluation of the time traces by counting the length of binding events directly yielded the dwell time histogram of NTF2 binding to the NPC (see Materials and methods and Online supplemental material). The obtained dwell time histogram was based on the observation of 335 independent binding events at the NE (Fig. 5 D). Fitting the histogram data by a single exponential yielded a satisfying description of the dissociation kinetics of bound NTF2-

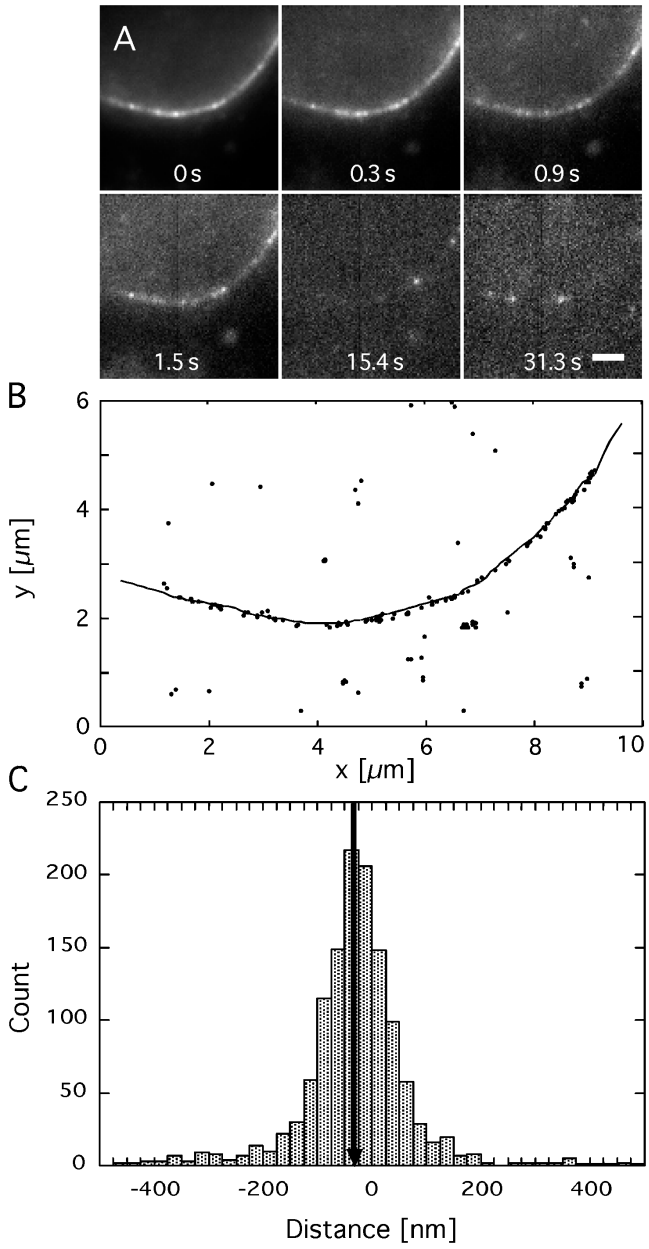

Figure 4. **Individual NTF2-Alexa488 molecules observed at the NE.** (A) The equatorial plane of a HeLa cell nucleus was imaged and bleached in the green channel in the presence of picomolar concentrations of NTF2-Alexa488. Complete bleaching of the dominant GFP fluorescence was achieved within 1 s of continuous illumination with 2 kW/cm^2 of 488-nm laser light. Only then, the single, much fainter fluorescent NTF2 molecules became visible. The shown frames are video stills taken with a frame integration time of 50 ms at the indicated time points (see Video 1, available at http://www.jcb.org/cgi/content/full/jcb.200411005/DC1). All frames were contrasted to fluorescence minimum and maximum within each frame; absolute intensities were 2927, 633, 311, 212, 120, and 86, respectively. Bar, 2 μm. (B) Position of the GFP-POM121 (solid line) and all NTF2 molecules observed in the image sequence (dots). Numerous molecules bind at identical, putative NPC positions. (C) NTF2-Alexa488 binding site distribution in relation to GFP-POM121. The long frame integration time prevented frequent observations of single NTF2-Alexa488 molecules in the nuclear interior.

Published January 18, 2005

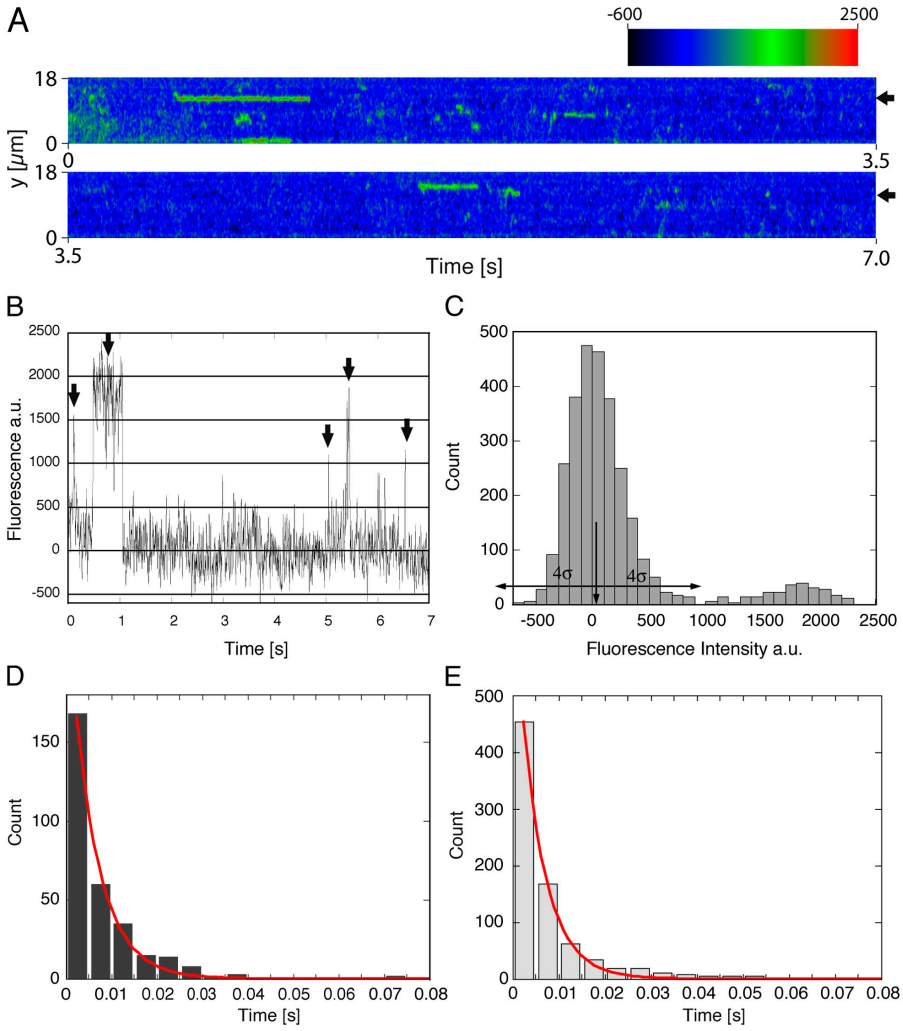

Figure 5. **Binding duration of NTF2 at the NPC.** The original video data is shown in Video 2 (available at http://www.jcb.org/cgi/content/full/jcb.200411005/DC1). (A) The line of fluorescence intensities along the NE—averaged over three adjacent pixels—was plotted as a function of time. The bright lines in the image indicate the transient binding of single NTF2 molecules to the NE. (B) Fluorescence intensity along one row in A as a function of time (A, arrows on the right-hand side). The arrows indicate binding events at this NE position. (C) Frequency distribution of the fluorescence intensities of the time trace. The distribution showed two distinct maxima corresponding to the unbound state, when no NTF2-Alexa633 was present at the selected NE site, and bound states. The unbound state corresponded to the background signal distribution and was fitted by a Gaussian. A threshold was defined by the mean value plus 4 × SD. All intensity values above this threshold were interpreted as binding events (B, arrows). (D) Evaluation of such time traces yielded the dwell time histogram of NTF2 binding. The histogram data were fitted by an exponential describing the dissociation of bound NTF2-Alexa633 molecules from the NPC yielding a time constant of $\tau_{NTF2} = 5.8 \pm 0.2$ ms. (E) Histogram of the binding times from experiments using NTF2-Alexa633 complexed with RanGDP. The corresponding fit yielded $\tau_{NTF2\text{–}RanGDP} = 5.2 \pm 0.2$ ms.

Alexa633 molecules from the NPC with a time constant of $\tau_{NTF2} = 5.8 \pm 0.2$ ms (Table I). In addition, we repeatedly observed significantly longer dwell times extending over hundreds of milliseconds (e.g., Fig. 5 B). Approximately 6.2% (21 out of 335) of all observed dwell times were longer than 100 ms. The long dwell times are also documented in Video 1, which was recorded with a frame rate of 6.7 Hz.

The dwell time of the NTF2-RanGDP complex is shorter than that of NTF2

NTF2 is the transport receptor for RanGDP (Ribbeck et al., 1998; Smith et al., 1998; Stewart et al., 1998). Therefore, we investigated whether or not the dwell time of NTF2 was altered by binding to its transport substrate. We performed experiments exactly as in the previous paragraph, with the only modification of adding 1 μM RanGDP. Under these conditions, each NTF2 molecule should be bound to RanGDP. Image acquisition and data analysis were performed in the same manner as before, and a corresponding dwell time histogram was obtained (Fig. 5 E). A monoexponential fit to the dwell time histogram revealed a time constant of $\tau_{NTF2\&RanGDP} = 5.2 \pm 0.2$ ms, slightly shorter than NTF2 alone. Please note that the measurements of τ_{NTF2} and $\tau_{NTF2\&RanGDP}$ were based on several hundred single binding events each, and therefore display very

Table I. **Results of the single-molecule dwell time analysis**

Molecule	Molecular mass	Number of analyzed binding events	Dwell time	Binding events longer than 100 ms
	kD		*ms*	*%*
NFT2 (dimer)	29.5	335	5.8 ± 0.2	6.2
NFT2–RanGDP (dimer)	83.6	828	5.2 ± 0.2	2.5
Transportin	97	296	7.2 ± 0.25	2.4
Transportin–M3-GST[a]	179	334	5.6 ± 0.2	1.5

[a]M3-GST occurred as dimer due to the action of GST, which forms homodimers. The given molecular mass is that of M3-GST dimer coupled to transportin.

Published January 18, 2005

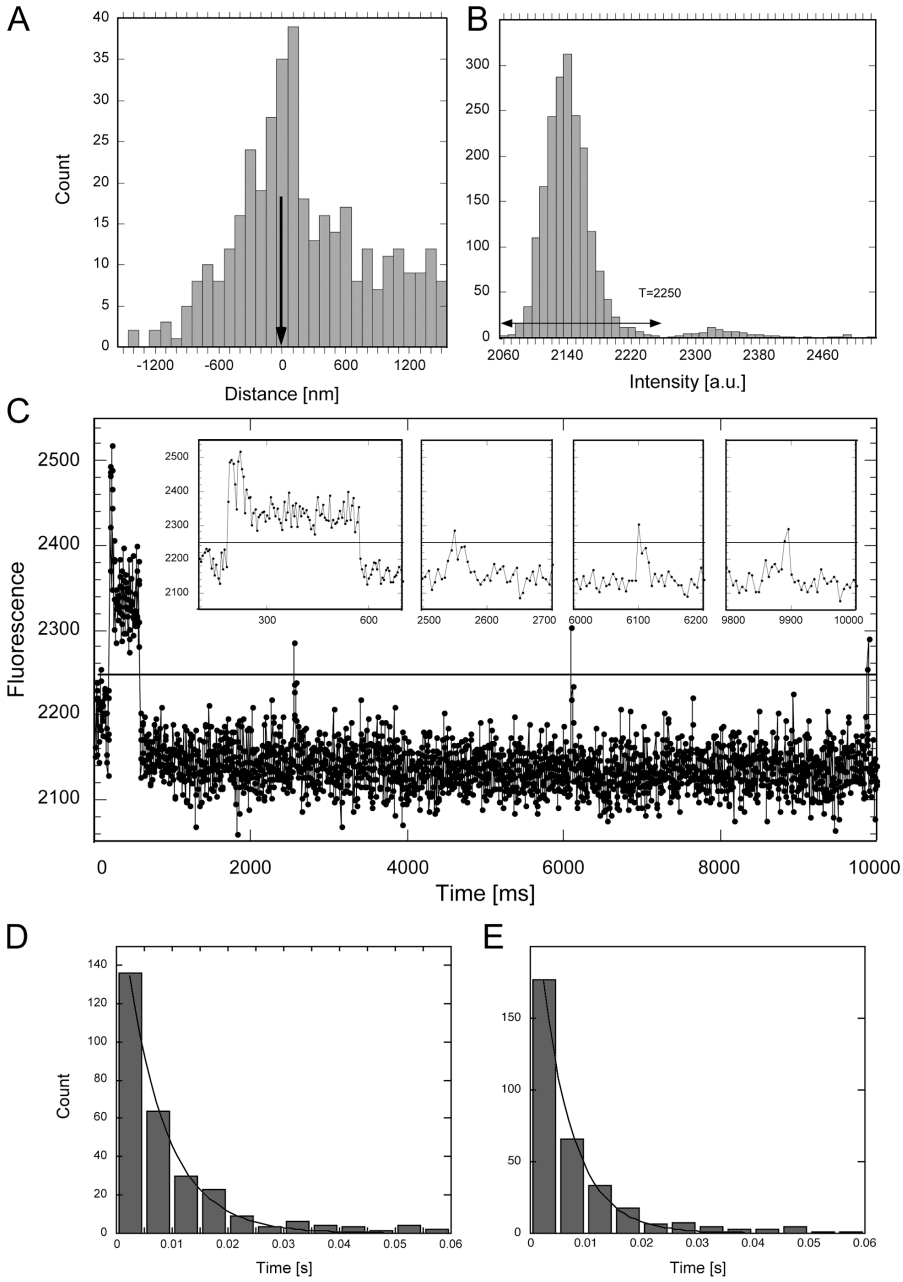

Figure 6. **Binding of transportin-Alexa633 to the NE.** (A) Binding site distribution of transportin in relation to GFP-POM121 from a single experiment. The mean of all positions determined between −300 and +300 nm was −2 nm (arrow). (B) Frequency distribution of the fluorescence intensities of the time trace shown in C. The distribution showed three distinct maxima corresponding to the unbound and bound states. The threshold was defined as described in the legend to Fig. 5. (C) Fluorescence intensity at one site on the NE plotted as a function of time. Binding events at this NE position are indicated by a fluorescence value above the threshold (horizontal line at 2250). (insets) Four binding events are shown at higher time resolution. The first inset shows a transportin molecule, which was probably labeled by two dye molecules as indicated by the successive bleaching yielding two distinct fluorescence levels of the bound state (B). The binding events were evaluated with regard to their duration, thus yielding the dwell time histogram of transportin-Alexa633 (D). The histogram data were fitted by an exponential yielding a time constant of $\tau_{transportin} = 7.1 \pm 0.2$ ms. (E) Histogram of the dwell times from experiments using transportin-Alexa633 complexed with M3-GST yielding $\tau_{transportin\&M3\text{-}GST} = 5.6 \pm 0.2$ ms.

small SEMs in the range of 0.01 ms. For that reason, there was a clear indication of a reduction in the NTF2 dwell time at the NE from 5.8 to 5.2 ms, when the receptor had bound its cargo. Notably, in this case also the fraction of long binding events (threshold 100 ms) was reduced from 6.2 to 2.5% (21 out of 828 total observations).

The dwell time of transportin 1 is longer than that of NTF2 but also reduced upon binding to its substrate

Transportin 1, a 97-kD protein also designated as karyopherin β2, is the transport receptor of the heterogeneous nuclear ribonucleoprotein A1 protein containing an NLS termed M9 (Nakielny et al., 1996). We used a peptide designated as M3 as import substrate. M3 comprises an M9-NLS conjugated to GST with a dimeric molecular mass of 82 kD (Chook et al., 2002). The experiments image acquisition and data analysis were performed similarly to the NTF2 experiments. Original data obtained at a frame rate of 200 Hz is shown in the Online supplemental material (Video 3, available at http://www.jcb.org/cgi/content/full/jcb.200411005/DC1). The video demonstrated that transportin molecules were detected predominantly at the NE, but could also be observed during their random movement within the cell nucleus due to the high time resolution of the observation. It could clearly be observed how the molecules were roaming the nucleus (Phair and Misteli, 2000) and were hitting binding sites from time to time. This finding could not be perceived in Video 1, which showed the transport of NTF2-Alexa488 at the significantly lower time resolution of 6.7 Hz (integration time 50 ms; see also Fig. 4 C). This was because the mobility of the molecules within the cell was so high that they could not be observed at the low time resolution, which

Published January 18, 2005

was used in the case of NTF2-Alexa488 in order to obtain an optimal localization precision during the binding at the NE. Only at the NE the molecules were localized for longer periods, thus giving rise to signals of sufficient intensity, otherwise the signals were too blurred for a confident detection. Fig. 6 A quantifies the resulting positions of the detected transportin molecules in terms of their distance distribution to the NE. The frequent observation at the NE was shown by the peak of the distribution at $d = -2$ nm, and the numerous molecules within the nucleus caused the shoulder at the right-hand side of the distribution. Fig. 6 C shows a time trace of one position at the NE over a time span of 10 s. During this time span, four transportin molecules bound to this site at the NE. The insets in Fig. 6 C show these events on an expanded time scale. In the first inset, long binding was most likely due to a transportin labeled by two dye molecules because the trace contains two distinct levels of fluorescence (Fig. 6 B, first inset). However, one dye molecule was bleached subsequent to some blinking after ~10 frames. Such blinking events are clear indications for the observation of single-molecule fluorescence (Kubitscheck et al., 2000). From such time traces, the corresponding dwell time histogram was obtained, again showing an approximate monoexponential decay behavior (Fig. 6 D). A monoexponential fit to the dwell time histogram of transportin 1 revealed a time constant of $\tau_{transportin} = 7.2 \pm 0.25$ ms, which was clearly longer than for NTF2. In the next experiments, the transport substrate M3-GST was added at the same concentration as transportin. The dwell time for the complex of receptor and substrate, $\tau_{Transportin\&GST\text{-}M3}$, was determined as 5.6 ± 0.2 ms, clearly shorter than the receptor alone. Again, the reduced binding duration was also reflected by a decreased number of long binding events. For transportin alone, 2.4% (7 out of 296 total observations) of the binding events were longer than 100 ms, whereas for transportin bound to GST-M3, the number of long binding events was reduced to 1.5% (5 out of 334 total observations).

Discussion

In this work, we used single-molecule fluorescence microscopy for the study of the topography and kinetic processes of supramolecular protein complexes deep within the interior of permeabilized cells. We found that the topography of the NPC could be resolved in its axial direction with high precision by single-molecule microscopy and measured the distance between the nucleoporins Nup358 and POM121. This introductory experiment established that the binding of single molecules to a supramolecular complex buried within a eukaryotic cell can unambiguously be analyzed by dual-color single-molecule microscopy with astonishingly high precision. However, such measurements require that the respective target epitope is readily accessible by the used positional probes and that nonspecific binding is negligible compared with specific binding. Next, we used the high localization precision to study the distribution of binding sites for the nuclear transport receptor of RanGDP, namely NTF2. Finally, we measured the dwell times of the import receptors NTF2 and transportin without and with respective specific cargo molecules at the NPC with millisecond time resolution. It seems that such kinetic measurements at the intact NPC are feasible only by single-molecule methods.

Single NTF2 molecules were most often detected directly at the NE. 77% of all molecules observed in a range of ±500 nm from the NE were found in the range of $-100 \text{ nm} \leq x \leq 75$ nm. The maximum of the binding site distribution was slightly shifted to the cytoplasmic side ($d = -30$ nm), with a very symmetrical appearance featuring a FWHM of only 125 nm, a value well below the optical resolution. This distribution suggested that NTF2 binding sites occur not only on the cytoplasmic filaments and at the cytoplasmic face of the central framework of the NPC but also within the central framework and on the proximal part of the nucleoplasmic filaments. However, it appears unlikely that there are many binding sites on the distal part of the nuclear filaments including the distal ring. These results corroborated the findings of a previous electron microscopic study, where gold-labeled NTF2 were shown to bind along the interior and the proximal part of the nuclear filaments of the NPC (Bayliss et al., 1999).

The dwell times of NTF2 without and with cargo were $\tau_{NTF2} = 5.8 \pm 0.2$ ms and $\tau_{NTF2\text{–}RanGDP} = 5.2 \pm 0.2$ ms, respectively. These numbers were based on the observation of hundreds of single binding events, and therefore have a correspondingly high precision. They indicate a slight decrease in binding duration if the cargo is bound to its receptor (Table I). This observation was even more obvious in the case of transportin, which was analyzed without and with a cargo peptide comprising an M9-NLS yielding dwell times of 7.1 ± 0.2 and 5.6 ± 0.2 ms, respectively.

The observation that the dwell time of both analyzed transport receptors was reduced upon binding to a specific transport substrate suggested that the overall transport speed for cargo-loaded receptors was accelerated in comparison to empty receptors. Clearly, the presence of the cargo decreased the interaction duration with the NPC, thus yielding higher translocation rates.

Analysis of the dwell times of the receptors without cargo in the context of the known translocation rates yields insights into the transport mechanism. For NTF2, Ribbeck and Görlich (2001) determined a transport rate of 2,500 NTF2-dimers/s/NPC at a concentration difference of 100 μM using permeabilized cells, and for the NPC of isolated *X. laevis* oocyte NEs we (Siebrasse and Peters, 2002) measured a rate of ~1,500 NTF2-dimers/s/NPC at a concentration difference of 14.8 μM. For transportin, Ribbeck and Görlich (2001) showed that single NPCs were able to translocate 800 transportin molecules/s at a concentration difference of 68 μM. Transport through a narrow channel containing single binding sites for the transport substrate on either face of the membrane can formally be described by saturation kinetics in analogy to Michaelis-Menten kinetics. In such a system, the maximal transport rate cannot be larger than the inverse of the mean dwell time. The dwell times measured by us could then only account for maximal transport rates of ~170 molecules/s/NPC for NTF2 and 140 molecules/s/NPC for transportin. Obviously, the bulk transport rates exceed these numbers by an order of magnitude. Hence, the binding process to the NPC itself does not present a rate-limiting step for the

Published January 18, 2005

overall transport. Rather, translocation through the NPC occurs simultaneously via multiple parallel pathways, as was recently also suggested by Yang et al. (2004). Considering the maximum bulk import rates for NTF2 and transportin per second and NPC, we can conclude that a single NPC may simultaneously harbor 15 empty NTF2 or 6 empty transportin molecules, respectively. With certainty, there is an abundance of FG repeats on the cytoplasmic filaments and the cytoplasmic side of the central framework, which can be occupied by FG repeat binding molecules in parallel. If that multitude of bound molecules is then passed one after the other through a short and narrow channel within the NPC at high speed, large residence times and high transport rates are obtained. Alternatively, one could speculate that transport takes place simultaneously along parallel pathways and binding sites within the transport channel. The first possibility corresponds to the suggestion by Rout et al. (2000), and the second comes close to that of Macara (2001). Macara (2001) assumes that the NPC contains a channel with a wall densely covered by FG repeats. Binding molecules would hop from one repeat to the other while inert molecules would diffuse through the open center of the channel. Rout et al. (2000) suggested that transport occurs via a channel traversing the center of the NPC. Binding sites at the channel entrance would facilitate the diffusion of binding molecules through the channel, whereas nonbinding molecules would be rejected by entropic exclusion, a mechanism referred to as "Brownian affinity gating." Ribbeck and Görlich (2001) proposed that the NPC center is occupied by a dynamic meshwork of FG repeats, acting as a "selective hydrophobic phase." Binding molecules would be dissolved in that phase and cross it by diffusion; nonbinding molecules would be excluded. This model is also compatible with the idea of several molecules being simultaneously translocated.

The fit of the dwell time histograms by a single exponential function yielded good, yet not perfect, agreement with the experimental data. In each single case, small deviations between data and fit were noticeable for dwell times of longer than 30 ms. Furthermore, in addition to the dwell times on the millisecond time scale, we observed for all substrates and complexes studied also binding events to NPCs, which lasted for hundreds of milliseconds. The probability to observe binding events for longer than 100 ms was between 2 and 6%, and was related to the dwell time in the millisecond range (Table I). These relatively high numbers are not compatible with the assumption of a single rate-limiting dissociation step. This result was in agreement with recent observations by Babcock et al. (2004). We could not yet resolve the nature of the longer binding events, possibly they were due to transport attempts through NPCs, which were clogged transiently by translocating RNP particles.

Our kinetic data allow another exciting speculation. A look at the dwell times of the empty receptors might suggest that they were related to their molecular mass (Table I). This hypothesis seems reasonable because more bulky molecules should need more time to move through the narrow pore and also because larger transport receptors may offer more interaction binding sites to the internal NPC sites. This hypothesis can be designated as "mass" effect. However, upon binding to their transport substrates, the dwell times were reduced. Apparently, the presence of the transport substrate reduced the number and/or durations of receptor interactions with NPC binding sites. This could be due to a steric "shielding" effect, which would counteract the mass effect. Notably, even the binding of transportin to M3-GST reduced the receptor dwell time, although the transportin–M3-GST complex had a noticeably higher molecular mass than transportin alone. In this case, the shielding effect was stronger than the mass effect.

Single-molecule microscopy allows completely new insights into the events at the supramolecular NPC because it can be applied in vivo and circumvents need of synchronizing a bulk of complexes in a specific kinetic state. We are confident that further real-time single-molecule studies will help to resolve the riddle of nucleocytoplasmic transport in the near future.

Materials and methods

Cell culture, reagents, and antibodies

A HeLa cell line stably expressing the GFP-conjugate of POM121 was provided by B. Burke (University of Florida, Gainesville, FL). A polyclonal mouse antibody against Nup358 (αNup358) was provided by E. Coutavas (Howard Hughes Medical Institute, The Rockefeller University, New York, NY). RanGDP was donated by I. Vetter (Max-Planck Institut für Molekulare Physiologie, Dortmund, Germany). Alexa Fluor 488 and 633 carboxylic acid, succinimidyl esters, Alexa Fluor 633–labeled anti–mouse and anti–rabbit antibodies (6.8 dye molecules per protein) were purchased from Molecular Probes. Human NTF2 was expressed, purified, labeled, and characterized as described previously (Siebrasse and Peters, 2002). Transportin I and GST-M3 were made according to Chook et al. (2002).

Experimental setup and fluorescence microscopy

Single molecule experiments were performed at RT using a wide-field single-molecule microscope (model Axiovert 100TV; Carl Zeiss MicroImaging, Inc.; equipped with a 63× NA 1.4 oil objective lens; Kues et al., 2001). The setup and the used image processing procedures are described in detail in the Online supplemental material.

Imaging of the NE

Cells were permeabilized with digitonin according to Adam et al. (1990). All experiments were performed in transport buffer (50 mM Hepes/KOH, pH 7.3, 110 mM potassium acetate, 5 mM sodium acetate, 2 mM magnesium acetate, 1 mM EGTA, and 2 mM DTT). A green fluorescent NE of a cell was searched, and the focus position was adjusted to the equatorial plane. After addition of the probe molecules, the sample was fine-focused in the green channel, and an image of the equatorial plane of the GFP-labeled envelope was recorded.

Imaging of single antibodies

Primary antibodies (αNup358) were added to the permeabilized cells and incubated for 30 min on ice. After washing, the coverslips were transferred to a custom-made sample holder and covered with buffer and a lid. Alexa633-labeled secondary antibodies were added at concentrations of 0.1 to 1 nM, depending on the actual cell density. Sequential image acquisition in the red channel was started immediately after acquisition of the green image and continued for 400 images.

Imaging of transport substrates

NTF2-Alexa633 was added at final concentrations of 0.2 nM to the permeabilized cells. After imaging the NE, videos taken in the red channel illustrated the binding of NTF2 to the NPCs. When using the Sensys camera (Photometrics) with an integration time of 50 ms, 400 images were obtained, whereas in experiments using the iXon camera (Andor Technologies) with integration times between 2 and 5 ms, up to 3,000 single frames were taken. In experiments using NTF2-Alexa488, imaging simultaneously photobleached the GFP-POM121. After GFP bleaching, single NTF2-Alexa488 fluorescence signals became perceptible at the NE.

All experiments were performed on three to six different cells of a single preparation, which were repeated at least threefold. Hundreds of single molecule signals were evaluated for each experimental condition.

Published January 18, 2005

Data analysis

All data analysis procedures are described in detail in the Online supplemental material. Programs were developed in C as macros or extensions to IPLab 3.2.4 (Scanalytics).

Image alignment

The green and red fluorescence channels were aligned using images of singly dispersed, immobilized multicolor microbeads (TetraSpeck Microspheres; 0.2 μm; Molecular Probes).

Position of the GFP-POM121

We acquired images of equatorial sections of cell nuclei that were oriented parallel to the y-axis or the x-axis. Before further processing, images were filtered using a 5 × 5 Gaussian kernel with an SD of 108 nm. A one-dimensional, nonlinear peak-fitting program, which approximated the fluorescence profile along the pixel rows or columns perpendicular to the envelope orientation by a Gaussian function on a linearly increasing background in a region of ±5 pixels around the maximum intensity, determined the maxima of the fluorescence profile with sub-pixel precision. The fluorescence maxima positions could be determined with a precision of better than 10 nm, because the signal/noise ratio was generally >20 (Kubitscheck et al., 2000).

Determination of single-molecule positions

Each image was background subtracted and smoothed with a 0.6-pixel Gaussian filter. The cross-correlation image with the point-spread function was calculated. The result was thresholded to yield segments, which represented regions of maximum overlap with the point-spread function. Their centers of mass were used to define centers of circular regions with a 7-pixel radius within the original image data. From these regions, the starting values for a nonlinear fitting procedure for a two-dimensional Gaussian function with constant background were extracted. The fitting routine determined position, width, amplitude, and background of the single-molecule signals in every frame. Single-molecule positions were determined with localization precisions between 20 and 40 nm with a mean of 22 nm.

Distance determination from NE

For each single-molecule position, we searched the two nearest positions of the NE, which were then connected by a linear line segment. The distance of the single-molecule position to the nearest point on that segment was defined as its distance to the NE. Interpolation errors were <1 nm.

Dwell time measurements

These measurements were performed using the high-speed iXon camera with a 128 × 128 pixel frame-transfer EMCCD. The CCD pixel size of 24 μm corresponded in object space to a size of 380 nm, which reduces the localization precision. Therefore, all single-molecule signals observed within a distance of ±1.5 pixels (±570 nm) from the NE were taken as being attached to the NPCs. They were visualized by averaging the intensities of three pixels on respective lines perpendicular to the NE and plotting the resulting one-dimensional intensity data along the NE as a function of time. The resulting yt-images were analyzed by searching for lines along the t-axis showing repetitive single-molecule binding events. Along these lines (corresponding to specific positions at the NE with putative NPC positions), we determined the histogram of fluorescence intensity values, which showed two distinct maxima, namely the background and the distinct intensity increase upon single molecule binding. The background intensities were fitted by a Gaussian, and a threshold was defined, which corresponded to the background average plus 4 × SD. All yt-positions with intensity values above the threshold were taken as indicating binding events. The duration of these events was determined from the corresponding fluorescence time traces. During image acquisition, molecules might have been bleached. Therefore, the determined dwell times represent lower limits.

Online supplemental material

The videos contained in the online supplemental material were prepared using IPLab and Quicktime 6 Professional. Video 1 was acquired with a frame integration time of 50 ms and a read-out time of 100 ms. The video data was not filtered and displayed in real time. The red channel of Video 2 was acquired with the EMCCD camera using a frame integration time of 2.5 ms at a frame rate of 400 Hz. The data were filtered with a 3 × 3 × 3 Gaussian kernel in x, y, and t, background-subtracted, and gamma-adjusted (1.5) before overlay with the green channel. The images of Video 3 were acquired with single frame integration times of 5 ms at a frame rate of 200 Hz. The video data were background-subtracted and gamma-adjusted (1.5) for display. Online supplemental material is available at http://www.jcb.org/cgi/content/full/jcb.200411005/DC1.

Grants from the VolkswagenStiftung and from the Deutsche Forschungsgemeinschaft to U. Kubitscheck and R. Peters are gratefully acknowledged.

Submitted: 1 November 2004
Accepted: 22 November 2004

References

Adam, S.A., R.S. Marr, and L. Gerace. 1990. Nuclear protein import in permeabilized mammalian cells requires soluble cytoplasmic factors. *J. Cell Biol.* 111:807–816.

Babcock, H.P., C. Chen, and X. Zhuang. 2004. Using single-particle tracking to study nuclear trafficking of viral genes. *Biophys. J.* 87:2749–2758.

Bayliss, R., R.K. Ribbeck, D. Akin, H.M. Kent, C.M. Feldherr, D. Görlich, and M. Stewart. 1999. Interaction between NTF2 and xFxFG-containing nucleoporins is required to mediate nuclear import of RanGDP. *J. Mol. Biol.* 293:579–593.

Bodoor, K., S. Shaikh, D. Salina, W.H. Raharjo, R. Bastos, M. Lohka, and B. Burke. 1999. Sequential recruitment of NPC proteins to the nuclear periphery at the end of mitosis. *J. Cell Sci.* 112:2253–2264.

Bonifaci, N., J. Moroianu, A. Radu, and G. Blobel. 1997. Karyopherin β2 mediates nuclear import of a mRNA binding protein. *Proc. Natl. Acad. Sci. USA.* 94:5055–5060.

Chook, Y.M., A. Jung, M.K. Rosen, and G. Blobel. 2002. Uncoupling Kapβ2 substrate dissociation and Ran binding. *Biochemistry.* 41:6955–6966.

Cordes, V.C., S. Reidenbach, H.-R. Rackwitz, and W.W. Franke. 1997. Identification of protein p270/Tpr as a constitutive component of the nuclear pore complex-attached intranuclear filaments. *J. Cell Biol.* 136:515–529.

Cronshaw, J.M., A.N. Krutchinsky, W. Zhang, B.T. Chait, and M.J. Matunis. 2002. Proteomic analysis of the mammalian nuclear pore complex. *J. Cell Biol.* 158:915–927.

Delphin, C., T. Guan, F. Melchior, and L. Gerace. 1997. RanGTP targets p97 to RanBP2, a filamentous protein localized at the cytoplasmic periphery of the nuclear pore complex. *Mol. Biol. Cell.* 8:2379–2390.

Fahrenkrog, B., and U. Aebi. 2002. The vertebrate nuclear pore complex: from structure to function. *Results Probl. Cell Differ.* 35:25–48.

Fahrenkrog, B., and U. Aebi. 2003. The nuclear pore complex: nucleocytoplasmic transport and beyond. *Nat. Rev. Mol. Cell Biol.* 4:757–766.

Hell, S., G. Reiner, C. Cremer, and E.H.K. Stelzer. 1993. Aberrations in confocal fluorescence microscopy induced by mismatches in refractive index. *J. Microsc.* 169:391–405.

Keminer, O., and R. Peters. 1999. Permeability of single nuclear pores. *Biophys. J.* 77:217–228.

Kiskin, N.I., J.P. Siebrasse, and R. Peters. 2003. Optical microwell assay of membrane transport kinetics. *Biophys. J.* 85:2311–2322.

Kubitscheck, U., P. Wedekind, O. Zeidler, M. Grote, and R. Peters. 1996. Single nuclear pores visualized by confocal microscopy and image processing. *Biophys. J.* 70:2067–2077.

Kubitscheck, U., O. Kückmann, T. Kues, and R. Peters. 2000. Imaging and tracking of single GFP molecules in solution. *Biophys. J.* 78:2170–2179.

Kuby, J. 1994. Immunology. W.H. Freeman and Company, New York. 670 pp.

Kues, T., A. Dickmanns, R. Lührmann, R. Peters, and U. Kubitscheck. 2001. High intranuclear mobility and dynamic clustering of the splicing factor U1 snRNP observed by single particle tracking. *Proc. Natl. Acad. Sci. USA.* 98:12021–12026.

Macara, I.G. 2001. Transport into and out of the nucleus. *Microbiol. Mol. Biol. Rev.* 65:570–594.

Michalet, X., A.N. Kapanidis, T. Laurence, F. Pinaud, S. Doose, M. Pflughoefft, and S. Weiss. 2003. The power and prospects of fluorescence microscopies and spectroscopies. *Annu. Rev. Biophys. Biomol. Struct.* 32: 161–182.

Moerner, W.E. 2003. Optical measurements of single molecules in cells. *Trends in Analytical Chemistry.* 22:544–548.

Moore, M.S., and G. Blobel. 1994. Purification of a Ran-interacting protein that is required for protein import into the nucleus. *Proc. Natl. Acad. Sci. USA.* 91:10212–10216.

Nakielny, S., M.C. Siomi, H. Siomi, W.M. Michael, V. Pollard, and G. Dreyfuss. 1996. Transportin: nuclear transport receptor of a novel nuclear protein import pathway. *Exp. Cell Res.* 229:261–266.

Paschal, B.M., and L. Gerace. 1995. Identification of NTF2, a cytosolic factor for nuclear import that interacts with nuclear pore protein p62. *J. Cell Biol.* 129:925–937.

Peters, R. 1986. Fluorescence microphotolysis to measure nucleocytoplasmic transport and intracellular mobility. *Biochim. Biophys. Acta.* 864:305–359.

Phair, R.D., and T. Misteli. 2000. High mobility of proteins in the mammalian cell nucleus. *Nature.* 404:604–609.

Pollard, V.W., W.M. Michael, S. Nakielny, M.C. Siomi, F. Wang, and G. Dreyfuss. 1996. A novel receptor-mediated nuclear import pathway. *Cell.* 86: 985–994.

Ribbeck, K., and D. Görlich. 2001. Kinetic analysis of translocation through nuclear pore complexes. *EMBO J.* 20:1320–1330.

Ribbeck, K., G. Lipowsky, H.M. Kent, M. Stewart, and D. Görlich. 1998. NTF2 mediates the nuclear import of Ran. *EMBO J.* 17:6587–6598.

Rout, M.P., J.D. Aitchison, A. Suprapto, K. Hjertaas, Y. Zhao, and B.T. Chait. 2000. The yeast nuclear pore complex: composition, architecture, and transport mechanism. *J. Cell Biol.* 148:635–651.

Sako, Y., and T. Yanagida. 2003. Single-molecule visualization in cell biology. *Nat. Rev. Mol. Cell Biol.* Suppl:SS1–SS5.

Schmidt, T., P. Hinterdorfer, and H. Schindler. 1999. Microscopy for recognition of individual biomolecules. *Microsc. Res. Tech.* 44:339–346.

Schütz, G.J., M. Sonnleitner, P. Hinterdorfer, and H. Schindler. 2000. Single molecule microscopy of biomembranes. *Mol. Membr. Biol.* 17:17–29.

Siebrasse, J.P., and R. Peters. 2002. Rapid translocation of NTF2 through the nuclear pore of isolated nuclei and nuclear envelopes. *EMBO Rep.* 3:887–892.

Smith, A., A. Brownawell, and I. Macara. 1998. Nuclear import of Ran is mediated by the transport factor NTF2. *Curr. Biol.* 8:1403–1406.

Söderqvist, H., G. Imreh, M. Kihlmark, C. Linnman, N. Ringertz, and E. Hallberg. 1997. Intracellular distribution of an integral nuclear pore membrane protein fused to green fluorescent protein—localization of a targeting domain. *Eur. J. Biochem.* 250:808–813.

Stewart, M., H.M. Kent, and A.J. McCoy. 1998. Structural basis for molecular recognition between nuclear transport factor 2 (NTF2) and the GDP-bound form of the Ras-family GTPase Ran. *J. Mol. Biol.* 277:635–646.

Suntharalingam, M., and S.R. Wente. 2003. Peering through the pore: nuclear pore complex structure, assembly, and function. *Dev. Cell.* 4:775–789.

Thompson, R.E., D.R. Larson, and W.W. Webb. 2002. Precise nanometer localization analysis for individual fluorescent probes. *Biophys. J.* 82:2775–2783.

van Oijen, A.M., J. Köhler, J. Schmidt, M. Müller, and G.J. Brakenhoff. 1998. 3-Dimensional super-resolution by spectrally selective imaging. *Chem. Phys. Lett.* 292:183–187.

Walther, T.C., H.S. Pickersgill, V.C. Cordes, M.W. Goldberg, T.D. Allen, I.W. Mattaj, and M. Fornerod. 2002. The cytoplasmic filaments of the nuclear pore complex are dispensable for selective nuclear protein import. *J. Cell Biol.* 158:63–77.

Wilken, N., J.L. Senecal, U. Scheer, and M.C. Dabauvalle. 1995. Localization of the Ran-GTP binding protein RanBP2 at the cytoplasmic side of the nuclear pore complex. *Eur. J. Cell Biol.* 68:211–219.

Wu, J., M.J. Matunis, D. Kraemer, G. Blobel, and E. Coutavas. 1995. Nup358, a cytoplasmically exposed nucleoporin with peptide repeats, Ran-GTP binding sites, zinc fingers, a cyclophilin A homologous domain, and a leucine-rich region. *J. Biol. Chem.* 270:14209–14213.

Yang, Q., M.P. Rout, and C.W. Akey. 1998. Three-dimensional architecture of the isolated yeast nuclear pore complex: functional and evolutionary implications. *Mol. Cell.* 1:223–234.

Yang, W., J. Gelles, and S.M. Musser. 2004. Imaging of single-molecule translocation through nuclear pore complexes. *Proc. Natl. Acad. Sci. USA.* 101:12887–12892.

Yildiz, A., J.N. Forkey, S.A. McKinney, T. Ha, Y.E. Goldman, and P.R. Selvin. 2003. Myosin V walks hand-over-hand: single fluorophore imaging with 1.5-nm localization. *Science.* 300:2061–2065.

Kubitscheck et al. http://www.jcb.org/cgi/doi/10.1083/jcb.200411005

Materials and methods

Experimental setup

An inverted wide-field epi-fluorescence microscope (model Axiovert 100TV; Carl Zeiss MicroImaging, Inc.; 63× NA 1.4 objective) was equipped with an Ar^+-laser (488 nm) and a HeNe-laser emitting at 633 nm. After passage through acousto-optical devices and λ/4-plates, both laser beams were coupled into an optical mono-mode fiber. The beam exiting the fiber was imaged into the object plane producing a Gaussian illumination profile with a full width at half maximum of 6 μm. The excitation intensity was to 1–2 kW/cm^2 per channel. Dual-color fluorescence was separated from the excitation light by a double dichromatic beam splitter (488/633 nm; Omega Optical Inc.). Fluorescence channels were separated by a dichromatic beam splitter (Dichroic BS XF 2016) and emission filters (green: α emitter XF 3084; red: custom α long pass filter, edge 645 nm), and recorded by cooled CCD cameras (green: Quantix with KAF 1400, pixel size 6.8 μm [Photometrics]; red: Sensys with KAF 1401e pixel size 6.8 μm [Photometrics], or iXon DV-860-BI, pixel size 24 μm, partly used in combination with a 4× magnifier [Andor Technologies]). Trigger signals generated by the cameras during image acquisition were used to switch the lasers on and off by the acousto-optical devices. QUANTIX and SENSYS images of were acquired with frame integration times of 50 ms, and iXon images were acquired with integration times of 2–5 ms. IPLab 3.2.4 (Scanalytics) was used to acquire the image data. Processing and analysis was performed as detailed below. For graphical presentation the images were mounted and overlaid using IPLab, final mounting was performed with Canvas 8, Adobe Illustrator 10, and Adobe Photoshop 7.

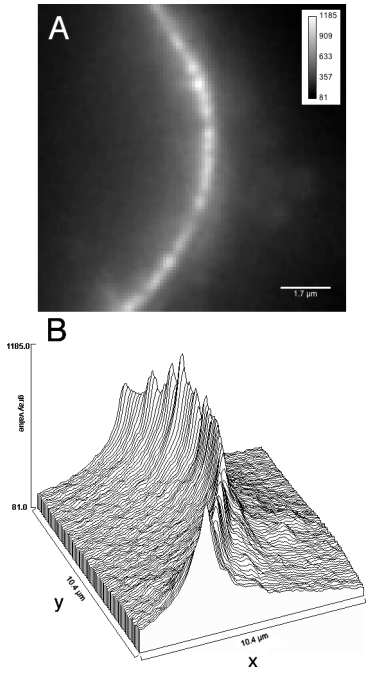

Figure S1. **Labeling of the NE by GFP-POM121.** (A) Bright-field image of the equatorial plane of HeLa cell nucleus. A line of green fluorescence originating from GFP-POM121 contained in the NPCs in focus marked the position of the NE. The image was smoothed by a Gaussian filter with an SD of 1 pixel, and contrasted for display. Field size, 10.8 × 10.8 μm^2. (B) Surface plot representation of A showing the excellent signal:noise ratio of the data.

Data analysis

Data analysis programs were written in the Macro Language of IPLab 3.2.4 on a Macintosh computer. The software employed for fitting the positions of single molecules and the NPC positions was programmed in C as extensions to IPLab using Metroworks Codewarrior IDE version 5.1.1.

Position of the GFP-POM121

We acquired images of equatorial sections of cell nuclei that were oriented approximately parallel to the y-axis or the x-axis as shown in Figs. 2 A, 3 A, 4 A, and 6 A. Prior to further processing, images were filtered using a 5 × 5 Gaussian kernel with an SD of 1 pixel (108 nm). Because the width of this Gaussian Kernel was below the optical resolution (≈250 nm), it served to reduce the image noise, and only negligibly distorted the images. It is difficult to estimate intensity values for all positions of the NE by visual inspection of the image data. To demonstrate the excellent signal:noise ratio of the image along the NE, we display a version of Fig. 2 B with calibration bar and an intensity surface plot (Fig. S1).

In the smoothed images, the position of the NE was determined as follows for the case of a NE being orientated along the y-axis. A maximum search routine was used to determine the brightest pixel for each row of pixels, designated as ($i_{max,j}$,j) in an approximately perpendicular direction to the NE. Using this pixel as starting position, we performed a fit of the one-dimensional profile along one row in a region of $i_{max} \pm 5$ pixels around the brightest pixel (e.g., Fig. S2) using a Gaussian function plus a linear background as approximation to the fluorescence distribution:

$$(x) = A + bx + Be^{-(x-x_0)^2/2\sigma^2}$$

where x denoted the pixel position. A, b, B, x_0, and σ were used as free parameters. The fit was based on minimization of the X^2-function using a Levenberg-Marquardt algorithm (Press et al., 1992). Data and fitting result along such a line are displayed in Fig. 2 B of the publication. Two further example regions are marked in Fig. S2. The results of the fitting procedure yielded NE positions for all lines j. In this manner, a line of points was determined, which represented the NPC positions along the NE. These discrete positions were linearly interpolated to obtain a continuous representation of the NE. To demonstrate that this approach is indeed able to find the NE even for NE segments, which are not perpendicular to either an image line or row (e.g., a position as marked by the arrow in Fig. S2), we determined the positions of a "known" NE. To this end, a theoretical NE image intensity distribution was calculated using Mathematica on the basis of a rotated Gaussian function with an SD of 2, a value corresponding to the experimental situation (see Fig. 2 B). The simulated nuclear envelope is shown in Fig. S2. Because the positions of the NE were exactly known in this image, they could be compared with the result of our NPC fitting routine. This was done in Fig. S3 for a NE segment, which was not parallel to the y-axis, namely from the uppermost region of Fig. S2. Here, the positions of the NE as calculated for every 0.1 pixels (circles) were interconnected by a spline fit. The squares mark the results of the NE determination routine, they were interconnected by straight lines. It is obvious that the systematic error of the

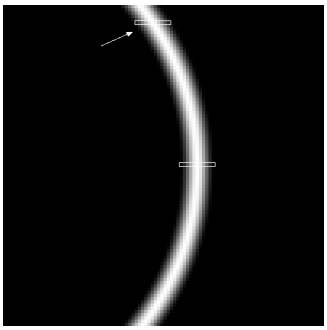

Figure S2. **Simulated profile of the NE.** To analyze the contributions of various sources of error, we worked with a simulated two-dimensional intensity profile of the NE. It was calculated on the basis of a rotated Gaussian function with an SD of 2, a value corresponding to the experimental situation.

one-dimensional peak-fitting approach was extremely small. Detailed analysis showed that the deviation between the true and the position as obtained from the linear interpolation of the fitting results was ≤0.025 pixels (<3 nm) as long as the angle between NE segment and y- respectively x-direction was below 45°.

The signal of the NE was very bright. This was due to the fact that relatively long image integration times were used for imaging (50–150 ms), that each NPC contains presumably several GFP molecules, and that often several NPC signals contributed due to the limited axial resolution. The signal:noise ratio at the NE position of the unfiltered images was usually >20. Based on the theory of Bobroff (1986), it can theoretically be deduced that in such a case the fluorescence maxima could be determined with a precision of ≤0.12 pixels corresponding to 13 nm (Kubitscheck et al., 2000). This theoretical prediction was verified by the repetitive imaging of a NE, and its subsequent localization according to the above procedure. Fig. S4 shows the distribution of deviations between the single measured positions and the respective mean position. As expected, the majority of deviations was indeed <10 nm (≈0.1 pixel), thus showing the excellent reproducibility of NE imaging and localization. The graph demonstrates also that the given localization precision is an average value. At some positions there exist also deviations of up to 30 nm. This occurred at (short) darker NE segments with a low GFP signal, where by chance no NPCs are present in the focal plane. Hence, the total error of the NE positions comprising the systematic deviation due to the line fits and the fitting precision was below 16 nm.

After single-molecule imaging a control image was taken in the green channel in order to check for any drift of the sample during the time of movie acquisition. If the control image indicated a total shift of the sample during the experiment of more than 50 nm, all data were discarded. This happened rarely, about in 1 out of 20 experiments.

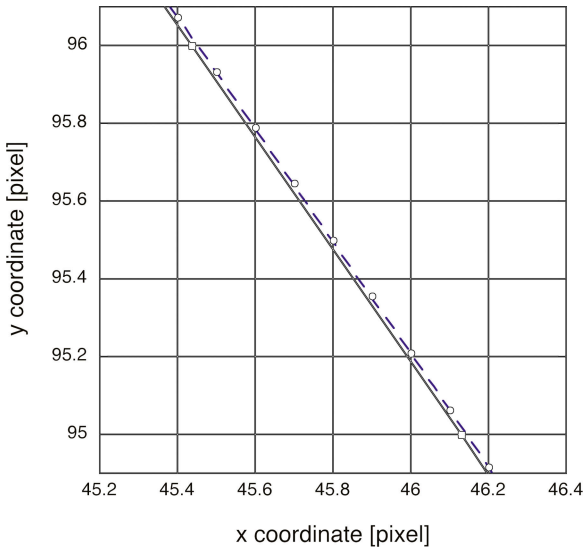

Figure S3. **Comparison between simulated NE position and fitting routine results.** The position of the simulated NE were exactly known, and calculated for every 0.1 pixels interconnected by a spline fit (circles) for an NE segment, which was not parallel to the y-axis, namely from the uppermost region marked in Fig. S2. The squares interconnected by straight line segments display the results of our NPC fitting routine and demonstrate the excellent agreement.

Determination of single-molecule positions

Single molecule signals were identified by a cross correlation approach. To this end, each image was background subtracted, and cross-correlation images with the point-spread function were calculated. The result was thresholded to yield segments, which represented regions of maximum overlap with the point-spread function.

The threshold was chosen by visual comparison of the raw data and the results of the peak-finding algorithm. The found signals were marked by image overlays with a size of 21 pixels each, and their center of mass was stored. Overlays of closely neighbored single-molecule signals fused, and had a total overlay size above 21. Such segments were sorted out. However, this happened quite rarely due to the low concentration of single molecules. The centers of mass of the segments defined the starting values for a nonlinear fitting procedure based on a two-dimensional Gaussian function with constant background, which was performed on the original image data. The fitting routine determined position, width, amplitude, and background of the single-molecule signals in every frame. Single-molecule positions could be determined with localization precisions between 20 and 40 nm (Kubitscheck et al., 2000).

Alignment of green and red positional data

The alignment of the images obtained in the two different fluorescence channels using two cameras introduced the largest uncertainty into the measurements. The green and red fluorescence channels were aligned using singly dispersed multi-color beads (TetraSpeck Microspheres 0.2 μm; Molecular Probes). These subresolution probes were immobilized on a coverslip, and imaged in both channels before and after cell measurements with a maximal time difference of 120 min. Bead positions were determined with precisions of <10 nm due to their high SNR using the same nonlinear fitting procedure, which was used for the single molecule. The positions of three or more single bead positions were determined in each channel. On the basis of these positions we determined the mathematical transformation (rotation followed by a translation), which mapped the green coordinate system onto the red. This transformation mapped the green bead positions with an average deviation of <10 nm onto the red bead positions. However, we detected a random movement of the two channels relative to each other, which caused an error in the alignment increasing with time to values of <200 nm within a time span of 120 min. The coordinate transformation, which was defined by the bead alignment, was applied to the NE position data posterior to the imaging process before the single molecule-NE distance analysis.

Distance determination from NE

As discussed above, the position of the NE was defined by a discrete set of coordinates denoting the row (column) number, and the result of the fitting process for each single row (column). For each single-molecule position we searched the two nearest points of the NE coordinate set, which were used to define a linear line segment. The lengths of these segments was <(108 nm √2). Considering the large radii of curvature of the cell nuclei, the linear interpolation between the NE positions was a very good approximation with a positional error of <5% of the segment length (corresponding to <10 nm). Finally the length of the perpendicular line segment from the point to the linear

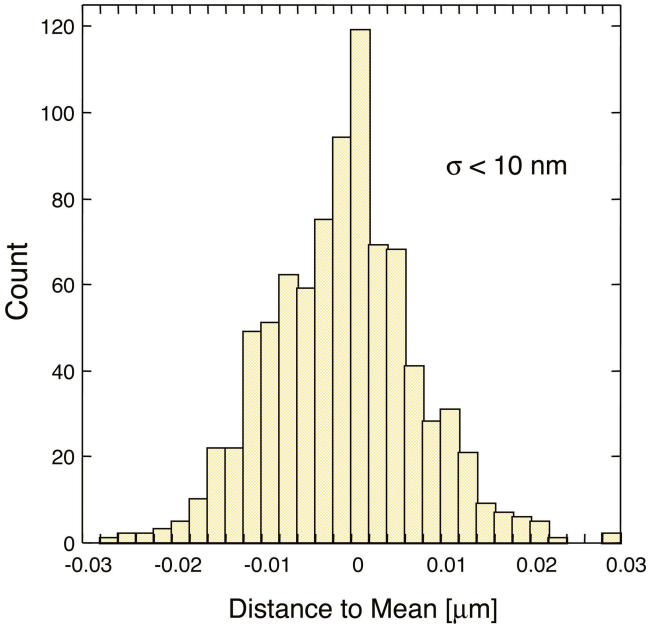

Figure S4. **Reproducibility of NE localization.** A fluorescent NE was imaged 10 times, and subsequently the NE was localized by the discussed fitting procedure. The graph shows a frequency histogram of the deviations between the single measured positions and the respective averaged position. The majority of deviations was indeed <10 nm (≈0.1 pixel), thus showing the excellent reproducibility of NE imaging and localization.

line segment connecting the two NE positions was defined as its distance to the NE. The final precision of this distance estimation can be obtained by Gaussian error propagation. Errors, which have to be considered, were discussed above, and are the (a) localization precision of the NE positions (<16 nm), (b) the error due to the linear approximation to the truly curved NE outline (<10 nm), (c) the localization precision of the single molecules (30 ± 10 nm), and (d) finally the error introduced by the image alignment procedure (<200 nm). All these errors limit the precision of a single distance measurement between single molecule and NE position to <205 nm, if two fluorescence channels are used. It should be noted that the determination of the average distance between single molecule positions and the NE can be determined with a significantly higher precision, because in that case the error has to be divided by the square root of the number of measurements. Furthermore, if the same channel was used for determination of envelope position and single-molecule positions (as was the case for NTF2-Alexa488), the error of a single measurement was reduced to <45 nm.

Dwell time measurements

These measurements were performed using the high-speed iXon camera with a 128 × 128 pixel frame-transfer EMCCD. The CCD pixel size of 24 μm corresponded in object space to a size of 380 nm. In the great majority of experiments, a 4× magnifying lens system was placed in front of the CCD, reducing the object space pixel size to 95 nm. To handle the vast amount of image data, the dwell times of the molecules binding to the NE were determined by the following data reduction procedure. The position of the NE was determined in the green reference image. Its position was copied as an image overlay—after the respective image alignment as described above—onto the red image data comprising the single molecule positions. Subsequently, only the region along the NE with a width of 3 or 5 pixels (depending on whether the magnifier was used for imaging or not) was evaluated in the red channel. In each frame the intensity values of the 3 respectively 5 pixel wide region were averaged over these pixels, thus reducing it to a single line data set. This line was now plotted as a function of time, thus revealing the events at the NE over the course of the experiment. Thereby an image was formed in which one dimension corresponded to the respective position on the line, and the second to time (Fig. 5 A). These yt- or xt-images were analyzed by searching for lines along the time axis showing repetitive single-molecule binding events. These lines corresponded to specific positions on the NE, which indicated with a great probability NPC positions. The time trace of such a position was shown in Fig. 5 B. At the corresponding positions in the red-channel data, we determined the histogram of fluorescence intensity values, which were measured over time. Typically these histograms displayed two distinct maxima, namely the background signal level and the distinct intensity increase upon single molecule binding (Fig. 5 C). The background intensities were fitted by a Gaussian function, and a threshold was defined, which corresponded to the background average plus four times the SD. Therefore, the observation of a higher intensity had a probability of <0.003%. Hence, all yt-positions with intensity values above the threshold were most probably due to binding events of fluorescent molecules. The duration of these events was determined from the corresponding fluorescence time traces. During image acquisition, molecules might have been bleached. Therefore, the determined dwell times represent lower limits. This procedure was tested by analyzing the time-dependent signals in arbitrary positions within nucleus or cytoplasm. Here, the detection of a single molecule event was extremely rare, and usually no correlated signal traces were obtained.

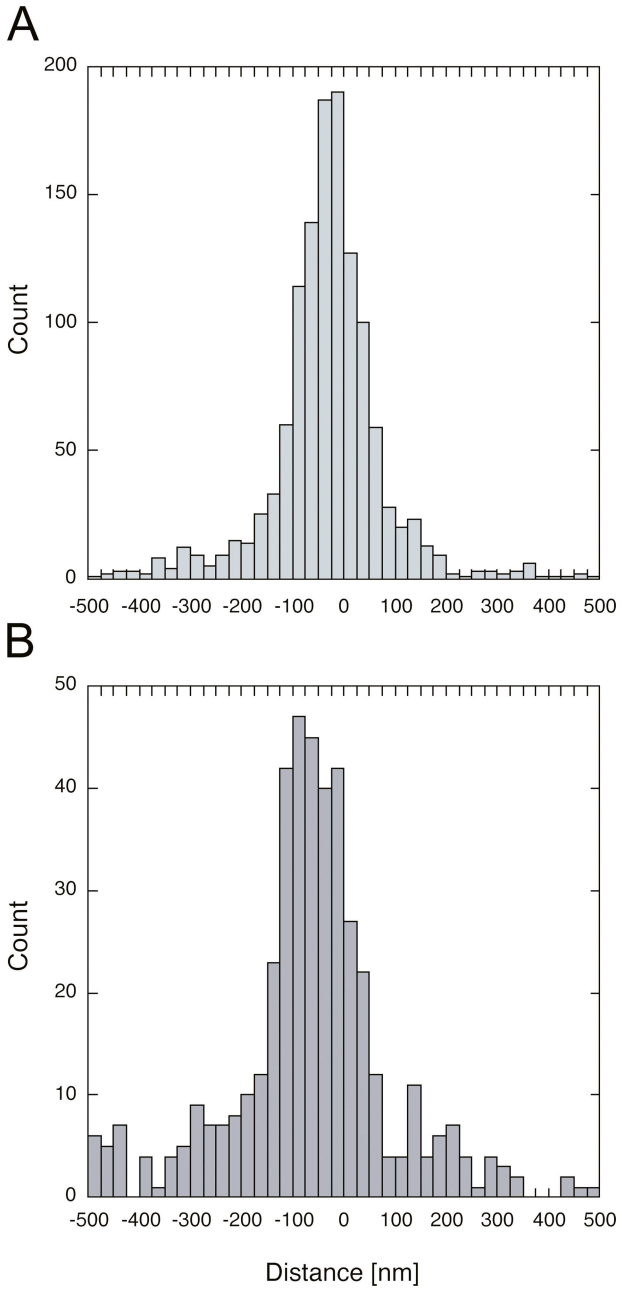

Figure S5. **Individual NTF2 molecules were observed at the NE.** (A) NTF2-Alexa488 binding site distribution in relation to GFP-POM121 (see Fig. 4C). (B) NTF2-Alexa633 binding site distribution in relation to GFP-POM121. The center of the distribution is only slightly shifted to the cytoplasm.

Supporting data

Transport of NTF2. The transport experiments with NTF2 were performed with molecules labeled by Alexa488 and also with further samples labeled by Alexa633. Data from the green-fluorescent NTF2-Alexa488 were shown in Fig. 4, which demonstrated the preferential observation of NTF2 directly at the NE. This was quantified in Fig. 4 C. A corresponding histogram obtained from experiments with Alexa633-labeled NTF2 is shown in Fig. S5. As in the case of Alexa488-labeled NTF2, the great majority of NTF2 molecules was detected immediately at the NE. The distribution of Alexa633-labeled NTF2 was not as narrow as that of Alexa488-labeled NTF2, a fact, which was certainly due to the lower colocalization precision of the dual color fluorescence approach as discussed above.

References

Bobroff, N. 1986. Position measurement with a resolution and noise-limited instrument. *Rev. Sci. Instrum.* 57:1152–1157.

Kubitscheck, U., O. Kückmann, T. Kues, and R. Peters. 2000. Imaging and tracking of single GFP molecules in solution. *Biophys. J.* 78:2170–2179.

Press. W., S.A. Teukolsky, W.V. Vetterling, and B.P. Flannery. 1992. Numerical Recipes in C. Cambridge University Press, Cambridge. 994 pp.